IEEE Access
Multidisciplinary | Rapid Review | Open Access Journal

Received 21 August 2022, accepted 4 September 2022, date of publication 8 September 2022, date of current version 16 September 2022.

Digital Object Identifier 10.1109/ACCESS.2022.3204998

RESEARCH ARTICLE

An Effective Source Number Enumeration Approach Based on SEMD

SHENGGUO GE, SITI NURULAIN BINTI MOHD RUM, HAMIDAH IBRAHIM, (Member, IEEE), ERZAM MARSILAH, AND THINAGARAN PERUMAL, (Senior Member, IEEE)
Faculty of Computer Science and Information Technology, Universiti Putra Malaysia, Serdang 43400, Malaysia
Corresponding author: Siti Nurulain Binti Mohd Rum (snurulain@upm.edu.my)

ABSTRACT In signal processing, empirical mode decomposition (EMD) first decomposes the received single-channel signal into several intrinsic mode functions (IMFs) and a residual, and then uses machine learning methods for source number enumeration. EMD, however, has an end effect that can undermine the accuracy of source number enumeration. To address this issue, this paper proposed a new EMD method named Supplementary Empirical Mode Decomposition (SEMD), which improved the accuracy by extending the signal length. The proposed method can be better applied to the modal parameter identification of non-stationary and nonlinear data in the engineering field. This method first identifies two candidate extreme points, which are the closest to the function value of the first extreme point near the endpoint. Then, on one side of the candidate point, it finds a waveform similar to that at the endpoint. Finally, the maximum and minimum points at each end of the signal will be added to extend the length of the signal. The added extreme points are candidate extreme points in similar waveforms. For the improved source number enumeration method based on SEMD, the instantaneous phase is obtained first by SEMD and Hilbert transform (HT). Then, the instantaneous phase feature is extracted to obtain a high-dimensional eigenvalue vector. Finally, the back propagation (BP) neural network is used to predict the number of sources. Experiment shows that SEMD can effectively restrain the end effect, and the source number enumeration algorithm based on SEMD has a higher correct detection probability than others.

INDEX TERMS Empirical mode decomposition (EMD), source number enumeration, end effect, supplementary empirical mode decomposition (SEMD), BP neural network.

I. INTRODUCTION

Research on array signal processing in the direction of arrival (DOA) estimation is vital and has been widely used in radar [1], sonar [2], communications [3], and other fields [4], [5]. The algorithms based on subspace are an integral part of DOA estimation algorithms. The multiple signal classification (MUSIC) algorithm proposed by Schmidt [6] is representative of these algorithms. The MUSIC algorithm first performs eigenvalue decomposition on the covariance matrix data obtained by the array. Then, high-precision DOA estimation is realized by using the principle that the signal subspace and the noise subspace are orthogonal to each other. Researchers have proposed to improve the MUSIC algorithm with methods such as the minimum norm method (MNM) [7], multi-dimensional MUSIC method [8], Root-MUSIC method [9], etc. These algorithms, however, require spectral peak search for all angles in the space, inevitably increasing the computational complexity of the algorithm and undermining practical applications. The estimation of signal parameters via rotational invariance techniques (ESPRIT) proposed by Roy and Kailath [10] overcomes this shortcoming. Compared with the MUSIC algorithm, the ESPRIT algorithm does not require spectral peak search, and provides the analytical solution required for the performance parameters to be estimated, thus reducing the computational complexity, and therefore, it is more conducive to hardware implementation in practical applications. These DOA estimation algorithms, however, can only be performed when the number of signal sources is known and their estimation would be inaccurate

The associate editor coordinating the review of this manuscript and approving it for publication was Wei Liu.

if the number of signal sources is wrong. Therefore, the estimation of the number of signal sources is the primary task of DOA estimation.

Early methods of estimating the number of signal sources were based on the method of hypothesis testing, but these methods may be affected by subjective behavior during manual settings. In order to avoid this problem, later researchers proposed estimation methods based on information theoretic criteria (ITC). Akaike information criterion (AIC) proposed by Wax and Kailath [11] is a representative of these algorithms. The AIC method has good estimation performance under a low signal-to-noise ratio (SNR), but the method is not consistent in estimation and performs poorly at high SNR and a large number of snapshots. Minimum description length (MDL) proposed by Wax and Ziskind [12] achieved consistent estimation, but it performs pooly at low SNR and a small number of snapshots. Later, researchers improved the source number estimation method based on ITC Guo *et al*. [13] proposed a new source number estimation method based on MDL, which uses the modified covariance matrix and its eigenvectors to replace the eigenvalues used to estimate the source number. A new decision variable with better anti-noise ability is obtained by a series of transformations on the snapshot vector and the feature vector. Experiment shows that this method can estimate coherent and incoherent sources and perform well at low SNR Mariani *et al*. [14] proposed a new penalty strategy for source number estimation based on ITC, which controls the probability of overestimation below a specified level and is suitable for source number estimation in small samples Zhao *et al*. [15] proposed the Efficient Detection Criterion (EDC) to improve the penalty function in the ITC. Based on the framework of MDL criterion, Jian-jian *et al*. [16] proposed a new MDL criterion by combining some features of eigenvalue distribution in the random matrix theory with the density of observed data.

Nevertheless, these source number estimation algorithms based on ITC can only be performed in white gaussian noise. Given that the noise is mostly coloured noise in real environment, it is more meaningful to research the source number estimation in the coloured noise environment.

Gerschgorin's disk estimation (GDE) proposed by Wu *et al*. [17] can estimate unknown array signals in the background of white gaussian and coloured noise. This method uses the larger disc radius of the signal source eigenvalue, and the smaller disc radius of the noise eigenvalue to estimate the number of sources. But the GDE method is vulnerable to human interferences because it needs to manually set the adjustment factor, and the estimation performance will be better only when the adjustment factor is properly selected. Therefore, this method is vulnerable to human factors. The Canonical Correlation Technique (CCT) proposed by Chen *et al*. [18] has better estimation performance than the GDE method at low SNR. This method obtains the signal number from the canonical correlation coefficients derived from the data received by two separate arrays Lu and Zoubir [19] proposed a two-step test procedure based on random matrix theory for source number estimation. This method utilizes the distribution information of eigenvalues. The first test is to select a threshold to distinguish the signal eigenvalues from the noise eigenvalues. Theoretically, the number of signal sources is underestimated when the SNR is low and the sample is small. In this case, the second step test becomes necessary, i.e., the maximum a posterior probability (MAP) test, with which, a special threshold is determined. Experiment shows that this method can correctly estimate the source number even when the sample size is small.

Higher order cumulants can restrain the Gaussian coloured noise, so researchers proposed an algorithm to estimate the source number based on fourth-order cumulants [20] Yang *et al*. [21] proposed a source number enumeration algorithm based on virtual array expansion. Combining the GDE method with the fourth-order cumulant, this method shows good estimation performance.

As artificial neural networks (ANN) [22] become more powerful, ANN-based source number estimation algorithms are becoming increasingly popular Rogers *et al*. [23] proposed a method for estimating the number of narrowband sources based on deep learning. This method designs a 15-layer deep neural network, which takes the covariance matrix of the spatially smoothed signal and its eigenvalues as input for training and testing. Experiment shows that this method has good estimation performance at low SNR Fan *et al*. [24] proposed a multipath features fusion network, which fused the spatial features of the array and the temporal features of the snapshots using the multi-scale scheme of the Feature Pyramid Network and the Path Augmentation Scheme of the Path Aggregation Network. Therefore, sufficient source information can be extracted and better estimation performance can be obtained in the real environment Hu *et al*. [25] proposed an independent source number estimation method based on the supervised learning convolutional neural networks (CNN). The input of this CNN is a mixed signal sequence. When the network has sufficient data for training, the number of unknown sources can be estimated, which prepares for blind source separation.

As a powerful time-frequency analysis method, EMD [26] is also used in some source number enumeration algorithms Pan *et al*. [27] proposed to use EMD to decompose the original signal into several IMFs, and then extract features from the instantaneous phase of each IMF component, and finally use support vector machine (SVM) to predict the number of signal sources. However, EMD has certain inherent defects such as end effect [28] and mode mixing [29], and the elimination of these defects will improve the performance of the source number enumeration algorithm. Ensemble Empirical Mode Decomposition (EEMD) [30] makes improvement based on the EMD method, which avoids the mode mixing phenomenon. This improved method introduces uniformly distributed white noise multiple times during decomposition, which suppresses the noise of the signal itself, thereby obtaining a more accurate upper and lower envelope. Further, Complementary Ensemble Empirical Mode Decomposition

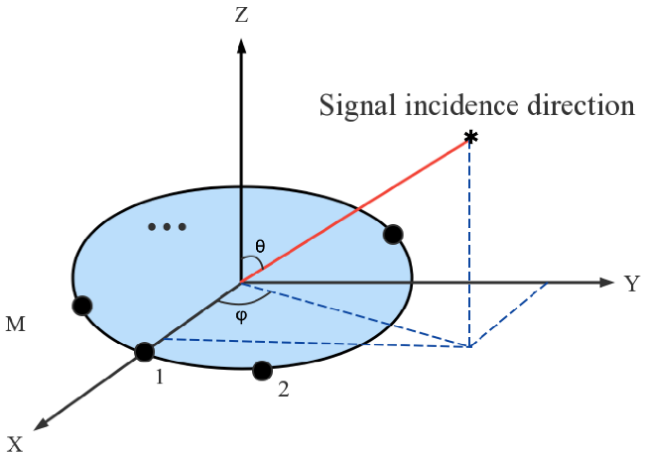

FIGURE 1. Array structure of the uniform circular array.

(CEEMD) [31] is an improved version of the EEMD method. It adds a pair of positive and negative white noises with opposite numbers to the source signal to eliminate the auxiliary white noise remaining after the decomposition of the EEMD method. The Local Mean Decomposition (LMD) method [32] can adaptively decompose a multi-component signal into a series of product functions (PF), where each PF is multiplied by a pure frequency modulation function and an envelope function. By combining the instantaneous frequencies and amplitudes of all PFs, the time-frequency distribution of the original signal can be presented. Although the LMD method is able to avoid the end effect, there is no significant improvement in mode mixing in EMD. The Variational Mode Decomposition (VMD) method [33] is adaptive and completely non-recursive. When obtaining the decomposed components, this method determines the frequency center and bandwidth of each component by iteratively searching for the optimal solution of the variational model, so that the signal components can be separated adaptively. Compared with EMD, VMD can effectively avoid the mode mixing and end effect in decomposition. This paper proposed a new method to restrain the end effect in EMD, and further proposed an improved source number enumeration algorithm.

The following content is organized as follows: Section II presents the relevant theoretical background. Section III discusses various application scenarios of the proposed SEMD method. Section IV introduced an improved source number enumeration method. Section V is the experiment and analysis of SEMD and the improved source number enumeration method. Finally, conclusions are given in Section VI.

II. THEORETICAL BACKGROUND

This section introduced the array signal model, the EMD method, and the BP algorithm.

A. SIGNAL MODEL

The uniform circular array (UCA) can obtain the azimuth and elevation angles of the signal source at the same time, and is often used for DOA estimation [34]. Therefore, this paper used a UCA with M array elements for source number enumeration. The array structure is shown in Fig. 1. The signal source is the Gaussian narrowband signal, and the wavelength is twice the radius of the UCA. Assuming that K far-field narrowband source signals are assumed to be incident with wavelength λ, azimuth angle θ, and elevation angle ϕ. The array signal mathematical model $X(t)$ of the t^{th} snapshot on M array elements is:

$$X(t) = [x_1(t), x_2(t), \ldots, x_M(t)]^T = AS(t) + K(t) \quad (1)$$

$$A = [a(\theta_1, \phi_1), a(\theta_2, \phi_2), \ldots, a(\theta_k, \phi_k)] \quad (2)$$

$$S(t) = [s_1(t), s_2(t), \ldots, s_K(t)]^T \quad (3)$$

$$K(t) = [k_1(t), k_2(t), \ldots, k_M(t)]^T \quad (4)$$

$$a(\theta_i, \phi_i) = [e^{j\phi_{i,1}}, e^{j\phi_{i,2}}, \ldots, e^{j\phi_{i,M}}]^T \quad (5)$$

$$\phi_{i,m} = \frac{2\pi r \sin(\theta_i)\cos(\phi_i - \frac{2\pi(m-1)}{M})}{\lambda}, \quad (m = 1, 2, \ldots, M) \quad (6)$$

where $X(t)$ is the output of M array elements; A is array manifold; $S(t)$ is the source vector; $K(t)$ is the additive noise; $a(\theta_i, \phi_i)$ is the steering vector; and (θ_i, ϕ_i) is the azimuth and elevation angles of the i^{th} signal source.

B. EMD

The EMD can be applied to nonlinear and non-stationary signals, with good self-adaptation [26]. In the decomposition process, the cubic spline interpolation method [35] is used multiple times to fit the upper and lower envelopes of the signal. The average of the upper and lower envelopes are taken to obtain several IMFs. Assuming that the signal $s(t)$ is composed of different IMFs, the specific decomposition process is as follows:

1) All the maximum and minimum points of the signal $s(t)$ are fitted to the upper envelope and the lower envelope respectively.
2) The mean value of the upper and lower envelopes are taken, and recorded as $m(t)$. The $h_1(t)$ can be obtained as:

$$h_1(t) = s(t) - m(t) \quad (7)$$

3) If meets the conditions of IMF, $h_1(t)$ will be the first IMF component of the $s(t)$. Otherwise, let $s(t) = h_1(t)$, then repeat the above steps until the first IMF component $c_1(t)$ is obtained.
4) After obtaining the first IMF component, the residual value sequence $r_1(t)$ can be obtained as:

$$r_1(t) = s(t) - c_1(t) \quad (8)$$

5) The above steps are repeated to obtain each IMF component: $r_n(t)$ is:

$$s(t) = \sum_{i=1}^{n-1} c_i(t) + r_n(t) \quad (9)$$

where $c_i(t)$ is the i^{th} IMF component and $r_n(t)$ is the residual component.

C. BP ALGORITHM

The BP neural network proposed by Rumelhart *et al.* [36] is capable of learning of the weights of the multi-layer neural network with the error back-propagation algorithm. For each neural unit in the hidden layer, the weights learning can approximate all non-mapping relationship, and has a strong nonlinear mapping ability. This algorithm includes two propagation processes, namely the forward propagation of the sample data and the back propagation of the estimation error. The specific process is as follows:

1) Initialize the BP neural network. Initial values are given for all values and thresholds in the neural network. Give a learning rate and the number of iterations. Pick a suitable excitation function.
2) The output of the hidden layer can be obtained by transforming the input parameters with the excitation function:

$$H_j = f(\sum_{i=1}^{n} w_{ij}x_i - a_j) \tag{10}$$

where f is the excitation function;w_{ij} is the weight between the i^{th} layer node and the j^{th} layer node; x_i is the i^{th} parameter of the input sequence; a_j is the threshold of the j^{th} layer node; and H_j is the output of the j^{th} layer, where $j = 1, 2, \ldots, l$.
3) For the output of each node in the output layer.H_j linear fitting is performed by the weightw_{jk} between the hidden layer node and the output layer node, and the threshold b_k of the output layer node. The output value O_k of the k^{th} node of the output layer can be obtained as:

$$O_k = \sum_{j=1}^{l} H_j w_{jk} - b_k, (k = 1, 2, \ldots, m) \tag{11}$$

4) Depending on the k^{th} ideal predicted value y_k and the k^{th} real output value O_k, the error can be obtained as:

$$e_k = y_k - O_k \tag{12}$$

III. SEMD

In order to restrain the end effect in EMD, this paper proposes the addition of the extreme points at both ends of the original signal to extend the signal length. This method uses the existing extreme points to predict the unknown extreme points, and then uses all the extreme points to obtain a new envelope curve. For a discrete signal $x(t)$, the time series of the signal is $\{t_1, t_2, \ldots, t_n\}$, and the signal sequence is $\{x(t_1), x(t_2), \ldots, x(t_n)\}$. Suppose the signal has B maximum points and L minimum points. The time of the maximum point is $T_M(i)(i = 1, \ldots, B)$, and the function value is $x_M(i)(i = 1, \ldots, B)$. The time of the minimum point is $T_N(j)(j = 1, \ldots, L)$, and the function value is $x_N(j)(j = 1, \ldots, L)$. The function value of the left endpoint of the signal is x_L and that of the right endpoint is x_R.

In order to extend the signal length, a maximum point and a minimum point are added to the left and right ends of the signal. The method first finds extreme points in the signal that are close to the function value of the first extreme point, and takes them as candidate extreme points. The slope of the two extreme points is used as an index to judge whether the two waveforms are similar. Then, on one side of the candidate point, the waveform that is the most similar to that on the left endpoint or the right endpoint is found. Finally, the extreme points in similar waveforms are the maximum and minimum points to be added. The specific method of adding extreme points is discussed as follows.

A. ADD EXTREME POINT AT LEFT END

1) Assuming that the first extreme point at the left end of the signal is the maximum point. The following definitions are available:

$$\begin{aligned} N_2 &= |x_M(1) - x_M(2)| \\ N_3 &= |x_M(1) - x_M(3)| \\ &\vdots \\ N_B &= |x_M(1) - x_M(B)| \end{aligned} \tag{13}$$

$$N_p = \min\{N_2, N_3, \ldots, N_B\} \tag{14}$$

$$N_q = \min\{N_2, N_3, \ldots, N_B\} \tag{15}$$

where $p \in \{2, 3, \ldots, B\}, q \in \{2, 3, \ldots, B\}$ and $q \neq p$. Therefore, the closest function values $x_M(1)$ are $x_M(p)$ and $x_M(q)$. Then, the extreme points where $x_M(p)$ and $x_M(q)$ located are selected as candidate maximum points. The waveform on the left side of the candidate extreme point is similar to that at the left endpoint. For the convenience of analysis, the function values of the minimum point on the left side of the candidate point are set as $x_N(u)$ and $x_N(v)$. Let the slopes of the straight lines between the extreme points of the function values $x_M(1)$ and x_L, $x_M(p)$ and $x_N(u)$, and $x_M(q)$ and $x_N(v)$ be k_1, k_2 and k_3. Set the function values of the maximum and minimum points added to the left end of the signal be $x_M(0)$ and $x_N(0)$, and the times are $T_M(0)$ and $T_N(0)$. The following derivation can be obtained:

$$F_1 = |k_1 - k_2| \tag{16}$$

$$F_2 = |k_1 - k_3| \tag{17}$$

$$\textit{If } \min\{F_1, F_2\} = F_1 :$$

$$T_N(0) = T_M(1) - (T_M(p) - T_N(u)) \tag{18}$$

$$x_N(0) = x_N(u) \tag{19}$$

$$T_M(0) = T_N(0) - (T_N(u) - T_M(p-1)) \tag{20}$$

$$x_M(0) = x_M(p-1) \tag{21}$$

$$\textit{If } \min\{F_1, F_2\} = F_2 :$$

$$T_N(0) = T_M(1) - (T_M(q) - T_N(v)) \tag{22}$$

$$x_N(0) = x_N(v) \tag{23}$$
$$T_M(0) = T_N(0) - (T_N(v) - T_M(q-1)) \tag{24}$$
$$x_M(0) = x_M(q-1) \tag{25}$$

2) Assuming that the first extreme point at the left end of the signal is the minimum point, the following definitions are obtained:

$$\begin{aligned} N_2 &= |x_N(1) - x_N(2)| \\ N_3 &= |x_N(1) - x_N(3)| \\ &\vdots \\ N_L &= |x_N(1) - x_N(L)| \end{aligned} \tag{26}$$
$$N_p = \min\{N_2, N_3, \ldots, N_L\} \tag{27}$$
$$N_q = \min\{N_2, N_3, \ldots, N_L\} \tag{28}$$

where $p \in \{2, 3, \ldots, L\}$, $q \in \{2, 3, \ldots, L\}$ and $q \neq p$. Therefore, the extreme points where the function values $x_N(p)$ and $x_N(q)$ are located are candidate minimum points. Set the function values of the maximum point on the left of the candidate point as $x_M(u)$ and $x_M(v)$. Set the slopes of the straight lines between the extreme points of the function values $x_N(1)$ and x_L, $x_N(p)$ and $x_M(u)$, and $x_N(q)$ and $x_M(v)$ be k_1, k_2 and k_3. Other parameters are defined and similarly to section (1). The following derivation is obtained:

$$F_1 = |k_1 - k_2| \tag{29}$$
$$F_2 = |k_1 - k_3| \tag{30}$$
$$\textit{If } \min\{F_1, F_2\} = F_1:$$
$$T_M(0) = T_N(1) - (T_N(p) - T_M(u)) \tag{31}$$
$$x_M(0) = x_M(u) \tag{32}$$
$$T_N(0) = T_M(0) - (T_M(u) - T_N(p-1)) \tag{33}$$
$$x_N(0) = x_N(p-1) \tag{34}$$
$$\textit{If } \min\{F_1, F_2\} = F_2:$$
$$T_M(0) = T_N(1) - (T_N(q) - T_M(v)) \tag{35}$$
$$x_M(0) = x_M(v) \tag{36}$$
$$T_N(0) = T_M(0) - (T_M(v) - T_N(q-1)) \tag{37}$$
$$x_N(0) = x_N(q-1) \tag{38}$$

B. ADD EXTREME POINT AT RIGHT END

1) Assuming that the first extreme point at the right end of the signal is the maximum point, the function value of this extreme point is $x_M(B)$. The following definitions are obtained:

$$\begin{aligned} N_1 &= |x_M(B) - x_M(1)| \\ N_2 &= |x_M(B) - x_M(2)| \\ &\vdots \\ N_{B-1} &= |x_M(B) - x_M(B-1)| \end{aligned} \tag{39}$$
$$N_p = \min\{N_1, N_2, \ldots, N_{B-1}\} \tag{40}$$
$$N_q = \min\{N_1, N_2, \ldots, N_{B-1}\} \tag{41}$$

where $p \in \{1, 2, \ldots, B-1\}$, $q \in \{1, 2, \ldots, B-1\}$ and $q \neq p$. Therefore, the closest function values $x_M(B)$ are $x_M(p)$ and $x_M(q)$. The extreme point where the function values $x_M(p)$ and $x_M(q)$ are located is selected as the candidate maximum value point. The waveform on the right side of the candidate extreme point is similar to the waveform at the right endpoint. Set the function values of the minimum point on the right side of the candidate point as $x_N(u)$ and $x_N(v)$. Set the slopes of the straight lines between the extreme points of the function values $x_M(B)$ and x_R, $x_M(p)$ and $x_N(u)$, and $x_M(q)$ and $x_N(v)$ lie as k_1, k_2 and k_3. Set the function values of the maximum and minimum values added to the right end of the signal as $x_M(B+1)$ and $x_N(L+1)$, and the time as $T_M(B+1)$ and $T_N(L+1)$. The following derivation can be obtained:

$$F_1 = |k_1 - k_2| \tag{42}$$
$$F_2 = |k_1 - k_3| \tag{43}$$
$$\textit{If } \min\{F_1, F_2\} = F_1:$$
$$T_N(L+1) = T_M(B) + (T_N(u) - T_M(p)) \tag{44}$$
$$x_N(L+1) = x_N(u) \tag{45}$$
$$T_M(B+1) = T_N(L+1) + (T_M(p+1) - T_N(u)) \tag{46}$$
$$x_M(B+1) = x_M(p+1) \tag{47}$$
$$\textit{If } \min\{F_1, F_2\} = F_2:$$
$$T_N(L+1) = T_M(B) + (T_N(v) - T_M(q)) \tag{48}$$
$$x_N(L+1) = x_N(v) \tag{49}$$
$$T_M(B+1) = T_N(L+1) + (T_M(q+1) - T_N(v)) \tag{50}$$
$$x_M(B+1) = x_M(q+1) \tag{51}$$

2) Assuming that the first extreme point at the right end of the signal is the minimum point, the function value of this extreme point is $x_N(L)$. The following definitions are available:

$$\begin{aligned} N_1 &= |x_N(L) - x_N(1)| \\ N_2 &= |x_N(L) - x_N(2)| \\ &\vdots \\ N_{L-1} &= |x_N(L) - x_N(L-1)| \end{aligned} \tag{52}$$
$$N_p = \min\{N_1, N_2, \ldots, N_{L-1}\} \tag{53}$$
$$N_q = \min\{N_1, N_2, \ldots, N_{L-1}\} \tag{54}$$

where $p \in \{1, 2, \ldots, L-1\}$, $q \in \{1, 2, \ldots, L-1\}$ and $q \neq p$. Therefore, the extreme points where the function values $x_N(p)$ and $x_N(q)$ are located at the candidate minimum points. Let the function values of the maximum point on the right side of the candidate

point be $x_M(u)$ and $x_M(v)$. Set the slopes of the straight lines between the extreme points of the function values $x_N(L)$ and x_R, $x_N(p)$ and $x_M(u)$, and $x_N(q)$ and $x_M(v)$ lie as k_1, k_2 and k_3. Other parameters are defined in the same way as section (1). The following derivation is obtained:

$$F_1 = |k_1 - k_2| \tag{55}$$
$$F_2 = |k_1 - k_3| \tag{56}$$
$$If\ \min\{F_1, F_2\} = F_1:$$
$$T_M(B+1) = T_N(L) + (T_M(u) - T_N(p)) \tag{57}$$
$$x_M(B+1) = x_M(u) \tag{58}$$
$$T_N(L+1) = T_M(B+1) + (T_N(p+1) - T_M(u)) \tag{59}$$
$$x_N(L+1) = x_N(p+1) \tag{60}$$
$$If\ \min\{F_1, F_2\} = F_2:$$
$$T_M(B+1) = T_N(L) + (T_M(v) - T_N(q)) \tag{61}$$
$$x_M(B+1) = x_M(v) \tag{62}$$
$$T_N(L+1) = T_M(B+1) + (T_N(q+1) - T_M(v)) \tag{63}$$
$$x_N(L+1) = x_N(q+1) \tag{64}$$

C. PROCESSING ENDPOINTS

If the function value at the end point is greater than that at the first maximum value point closest to the end point, or less than the first minimum value point, the endpoint will be outside the upper and lower envelopes. In order to avoid this situation, this type of point is taken as the first maximum or first minimum point closest to the endpoint. Then the above method is used to add a maximum value and a minimum value at both ends of the signal.

IV. SOURCE NUMBER ENUMERATION ALGORITHM

Reference [27] proposed a source enumeration based on a UCA in a determined case, while our work improved this method. First, the Hilbert-Huang transform (HHT) [37] is performed on the received signal to obtain the instantaneous phase. Notably, the HHT process is based on the SEMD proposed in this paper, not EMD. Then eigenvalue decomposition (EVD) [38] is performed on the covariance matrix of the instantaneous phase to obtain the eigenvalue vector. In addition, in order to obtain a high-dimensional eigenvalue vector, three different eigenvalues are added to the original eigenvectors. Finally, the designed BP neural network is trained for source number enumeration. The process of the source number enumeration algorithm is shown in Fig. 2.

A. GETTING THE SIGNAL INSTANTANEOUS PHASE

HHT has two processes, i.e. EMD and HT, which can process non-stationary nonlinear signals and obtain the instantaneous phase [37], but EMD has an end effect that can cause errors in the IMF components. The SEMD effectively restrains the end effect by extending the signal length. Therefore, this paper

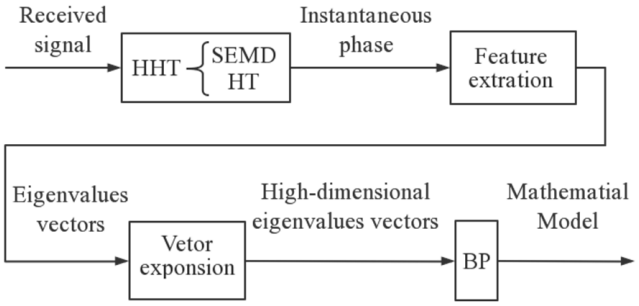

FIGURE 2. Flow chart of the source number enumeration algorithm.

uses a new HHT method combined with SEMD and HT. The spatial signal $s(t)$ received by the UCA model with M array elements is:

$$s(t) = [s_1(t), s_2(t), \ldots, s_M(t)] \tag{65}$$

It can be known from sections II.B and III that the signal $s_k(t)$ can be decomposed as:

$$s_k(t) = \sum_{i=1}^{n-1} c_{ki}(t) + r_{kn}(t) \tag{66}$$

where $k = 1, 2, \ldots, M$, $s_k(t)$ is the signal received on the k^{th} array element, $c_{ki}(t)$ is the i^{th} IMF, and $r_{kn}(t)$ is the residual. HT for each IMF is as follows:

$$H[c_{ki}(t)] = \frac{1}{\pi} p \int_{-\infty}^{\infty} \frac{c_{ki}(\tau)}{\tau - t} d\tau \tag{67}$$

where p is the Cauchy principal value. Then the instantaneous phase of $c_{ki}(t)$ can be expressed as:

$$\varphi_{ki}(t) = \arctan \frac{H[(c_{ki}(t))]}{c_{ki}(t)} \tag{68}$$

B. EXPANDING THE EIGENVECTORS

Wu and So [39] theoretically proved that due to the different positions of each array element in UCA, there will be phase differences when each array element receives the signal source. Therefore, the instantaneous phase can be used for feature extraction. First, the covariance matrix of the instantaneous phase between the array elements is constructed as follows:

$$\hat{\mathbf{R}}_i = \frac{1}{L} \Delta_i \Delta_i^T \tag{69}$$
$$\Delta_i = [\phi_{1i}, \phi_{2i}, \ldots, \phi_{Mi}]^T \tag{70}$$
$$\phi_{ki} = [\phi_{ki}(1), \phi_{ki}(2), \ldots, \phi_{ki}(L)] \tag{71}$$

where $i = 1, 2, \ldots, n-1$, L is the number of snapshots. Then do EVD on $\hat{\mathbf{R}}_i$ as:

$$\hat{\mathbf{R}}_i = \mathbf{U}_i \Lambda_i \mathbf{U}_i^T \tag{72}$$

where $\Lambda_i = diag(\lambda_{1i}, \lambda_{2i}, \ldots, \lambda_{Mi})$ is the eigenvalue. By calculating the correlation coefficient [40] between each IMF and the signal, it can be known that the first three IMFs have the largest correlation coefficient with the signal. Therefore,

the first three IMFs were selected for data analysis. With the above method being performed on the instantaneous phases of the first three IMFs, the $3 * M$ dimension eigenvalues can be obtained as follows:

$$(\lambda_{11}, \lambda_{21}, \ldots, \lambda_{M1}, \lambda_{12}, \lambda_{22}, \ldots, \lambda_{M2}, \lambda_{13}, \lambda_{23}, \ldots, \lambda_{M3}).$$

The signal is easily disturbed by the external environment, which will reduce the phase difference between the array elements. Therefore, this paper adds three different eigenvalues to highlight the phase difference between each array element. The 3*M dimensional eigenvalues are recorded as follows:

$$\lambda_1 \leq \lambda_2 \ldots \leq \lambda_{3M\text{-}1} \leq \lambda_{3M} \tag{73}$$

The three added difference eigenvalues are:

$$\lambda_{3M+1} = \lambda_{3M} - \lambda_1 \tag{74}$$
$$\lambda_{3M+2} = \lambda_{3M\text{-}1} - \lambda_2 \tag{75}$$
$$\lambda_{3M+3} = \lambda_{3M\text{-}2} - \lambda_3 \tag{76}$$

The eigenvalue vector after dimension expansion is:

$$\mathbf{T} = (\lambda_{11}, \ldots, \lambda_{(M+1)1}, \lambda_{12}, \ldots, \lambda_{(M+1)2}, \lambda_{13}, \ldots, \lambda_{(M+1)3})$$

All eigenvalues are normalized as:

$$\dot{\lambda}_i = \frac{\lambda_i}{\sum_{i=1}^{3*M+3} \lambda_i} \tag{77}$$

The normalized eigenvalue matrix is:

$$\mathbf{A} = (\dot{\lambda}_{11}, \ldots, \dot{\lambda}_{(M+1)1}, \dot{\lambda}_{12}, \ldots, \dot{\lambda}_{(M+1)2}, \dot{\lambda}_{13}, \ldots, \dot{\lambda}_{(M+1)3}) \tag{78}$$

C. THE NEURAL NETWORK SOURCE NUMBER ENUMERATION MODEL

A reasonable network structure can ensure high prediction accuracy, and in this work, the network model used is the BP neural network. Since the subsequent experiments in this paper use UCA with 4 array elements, signals with 1, 2, and 3 sources are enumerated respectively. Therefore, the number of nodes in the output layer of the network is 3, and the nodes in the input layer of the network are 15.

At present, there is no scientific method to determine the number of nodes in the hidden layer of the BP neural network. If the number of hidden layer nodes is smaller, the network iteration speed will be faster. Too few hidden layer nodes, however, can also affect the prediction accuracy of the network. This paper experimented many times and decided to use 2 hidden layers. First, the neural network with only one hidden layer is used for training. The more nodes in the hidden layer, the less error in the network decreases. A second hidden layer is added when the error of the network is minimized. The number of nodes in the first hidden layer is kept unchanged, and the number of nodes in the second hidden layer is increased until the entire network error minimizes. The structure of the final BP neural network is 15-17-6-3, as shown in Fig. 3.

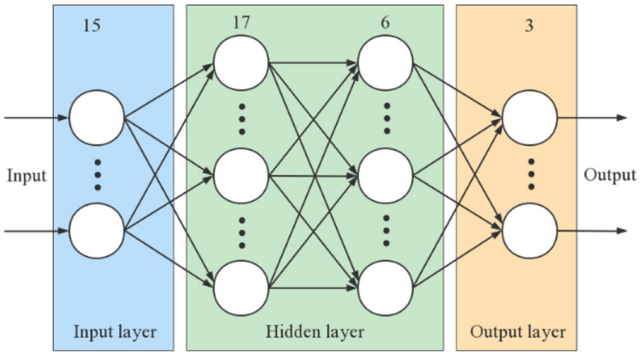

FIGURE 3. BP neural network structure.

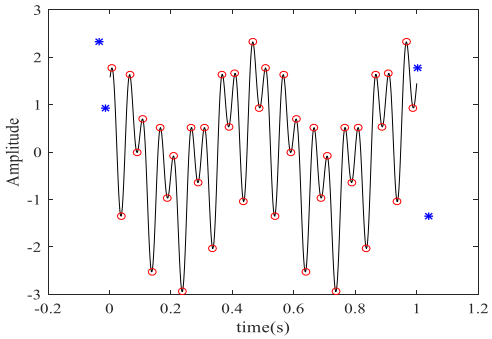

FIGURE 4. Distribution map of extreme value points based on SEMD.

V. EXPERIMENT AND ANALYSIS

This section verifies the effectiveness of SEMD in restraining the end effect by comparing the decomposition performance of EMD and SEMD. Then, the improved source number enumeration algorithm based on SEMD is evaluated based on computer data and radio frequency anechoic chamber data. Then, the experimental results of this method are compared and analyzed with other methods. The configurations of the computer used in this experiment are Intel i7 CPU and 16G memory, and the operating system is Microsoft Windows 10. The software used for data simulation is Matlab 2016a.

A. THE EFFECTIVENESS VERIFICATION OF THE SEMD

In order to verify the effectiveness of the SEMD method to restrain the end effect, this paper used a mixed signals to compare the algorithm performance of EMD and SEMD. The mixed signal $x(t)$ is:

$$x(t) = g(t) + h(t) + f(t) \tag{79}$$
$$g(t) = \sin(4\pi t + 2) \tag{80}$$
$$h(t) = \sin(40\pi t) \tag{81}$$
$$f(t) = \cos(20\pi t + 1) \tag{82}$$

First locate the extreme points of $x(t)$ is located. Then, a maximum point and a minimum point are added at both ends of the signal based on SEMD. As shown in Fig. 4, "$\circ$" represents the original extreme point of $x(t)$, and "$*$" represents the newly added extreme point.

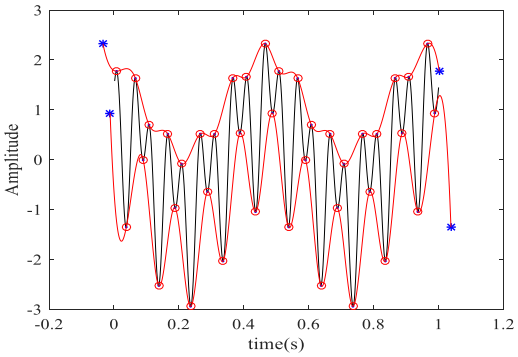

FIGURE 5. Upper and lower envelope fitting based on SEMD.

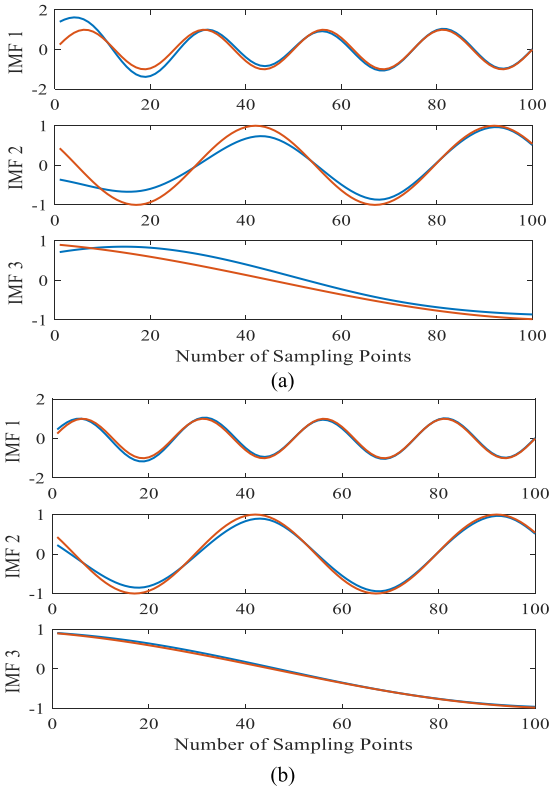

FIGURE 6. Signal decomposition diagram. (a) Based on EMD. (b) Based on SEMD.

Envelope fitting is performed on all maximum points and all minimum points by cubic spline interpolation. As shown in Fig. 5, the signal $x(t)$ is completely enveloped between the upper and lower envelopes, which indicates that the cubic spline interpolation based on SEMD can realize the full envelope of the signal.

The signal decomposition based on EMD and SEMD is shown in Fig. 6. In the figure, the blue and red lines represent the decomposed IMFs and the actual signal component, respectively. Compared with EMD, the IMF decomposed by CEMD is more consistent with the actual signal components, which is even more evident near the endpoints. This proves that SEMD can well restrain the end effect.

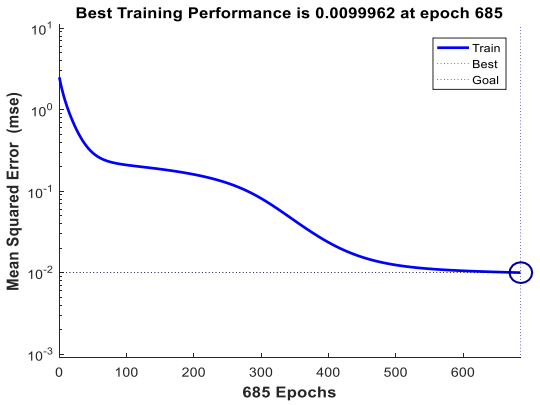

FIGURE 7. BP neural network training diagram.

B. THE SOURCE NUMBER ENUMERATION BASED ON COMPUTER DATA

In this paper, three far-field narrowband signals with one, two, and three sources are estimated by UCA with four array elements (4-UCA). The incident angles of the signal include the azimuth angles and the elevation angles. In order to train the BP neural network, three signals with SNR=15dB, L=200 and incident angles of (80°, 20°), (60°, 40°), (30°, 60°) are randomly selected, where L is the number of snapshots. The coloured noise contained in the signal is obtained by filtering the white gaussian noise [41]. 200 samples for each signal with one, two, and three sources are taken by the method in section IV. The samples of these three types of signals were labeled differently and then were mixed randomly into a dataset of 600 samples. This dataset is used to train the BP neural network, and the error accuracy is set to 0.01. As shown in Fig. 7, after 685 times of training, the network model reaches the error accuracy and the training is completed.

1) DETECTION PROBABILITIES AGAINST DIFFERENT SNRS

Set L=100, the SNR has a step size of 2 and values from −20dB to 20dB, 50 test samples are taken for each signal with one, two, and three sources and then were mixed randomly into a dataset containing 150 samples. It should be noted that the incident angle of the signal used in the training and test sample is different. The simulation results of this method are compared with the D-AIC method [42], the D-MDL method [42], the GDE method [43], the SORTE method [44] and the HHT-SVM method [27]. 100 Monte Carlo experiments were performed for each algorithm under different SNRs. Fig. 8 shows the detection probabilities of the six methods for signals with one source and three sources at different SNRs.

As can be seen from Fig. 8(a), except for the SORTE method and the GDE method, the detection probability of other methods has reached more than 90% in the entire SNR range. The detection probability of the proposed method all exceeds 95%, and the detection probability reaches 100% when SNR ≥ -12dB. As can be seen from Fig. 8(b), as the number of sources increases, the detection probability of the

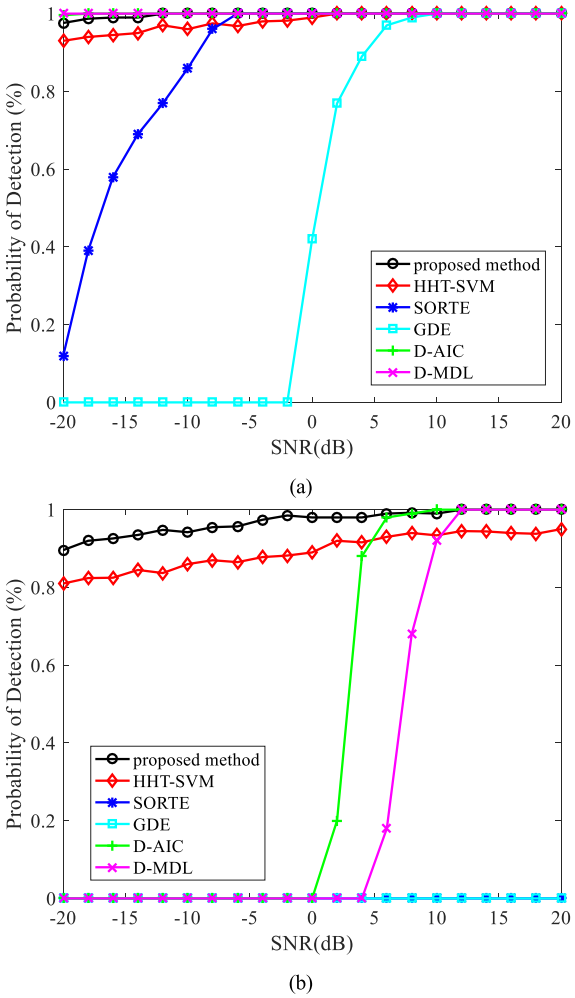

FIGURE 8. The detection probabilities of the six methods at different SNRs. (a) One source. (b) Three sources.

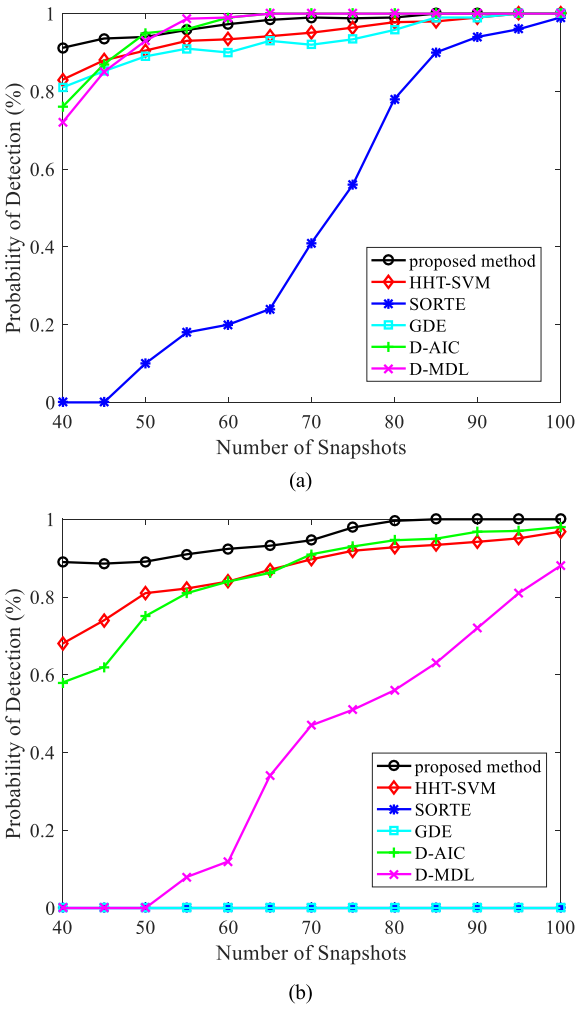

FIGURE 9. The detection probabilities of the six methods at different snapshots. (a) One source. (b) Three sources.

six methods decreases. The SORTE method and the GDE method have completely failed when the number of signal sources is three and the detection probability is zero. The detection probability of the D-AIC and D-MDL methods is zero at low SNR. Both the proposed method and the HHT-SVM method have good performance, but the detection rate of the proposed method in this paper is higher than that of the HHT-SVM method in the whole SNR range. According to the above analysis, when the number of sources increases, the proposed method has better performance than other methods under different SNRs.

2) DETECTION PROBABILITIES AGAINST DIFFERENT NUMBER OF SNAPSHOTS

Set SNR = 200dB, the L has a step size of 10 and the value is from 40 to 100. 100 Monte Carlo experiments are carried out for each method under different snapshot numbers, and other requirements are the same as in section (1). Fig. 9 shows the detection probabilities of the six methods for signals with one source and three sources at different snapshots.

As can be seen from fig. 9(a), except for the SORTE method, the detection probability of other methods increases rapidly with the increase of the snapshots number. Compared with other methods, the proposed method performs better when the number of snapshots is less than 50dB. It can be seen from fig. 9(b) that the SORTE and the GDE methods failed. The detection probability of the other four methods has also decreased compared with fig. 9(a). By contrast, the performance of the proposed method is better than other methods in the whole range of snapshot number, especially under the small number of snapshots.

C. THE SOURCE NUMBER ENUMERATION BASED ON RF ANECHOIC CHAMBER DATA

This paper used the signal data collected in the RF anechoic chamber to verify the performance of each method in a real environment. The parameters of the RF anechoic chamber are shown in Table 1.

Three signals with SNR = 20, L = 200, and incident angles of $(70°, 30°)$, $(50°, 40°)$, $(80°, 50°)$ are randomly

TABLE 1. Indexes of parameters in RF anechoic chambers.

Parameters	Index
RF anechoic chamber size	$6.4m \times 4.4m \times 5.5m$
VSG number	3
antenna number in UCA	4
transmitting antenna number	3
carrier frequency of RF signal	1561.092MHz
carrier frequency of observed signal	15.48MHz
signal bandwidth	1.5MHz
sampling frequency	62MHz
down conversion circuit bandwidth	20MHz

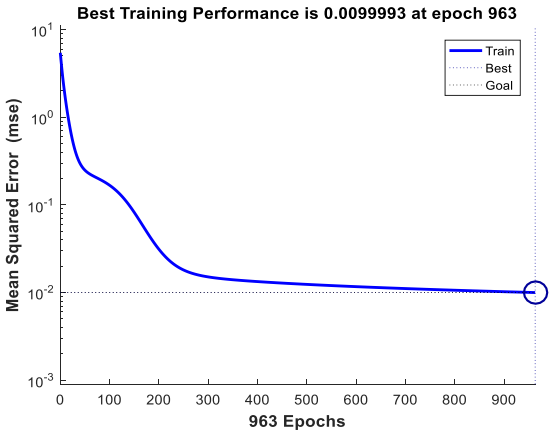

FIGURE 10. BP neural network training diagram.

selected. The RF anechoic chamber equipment is utilized to acquire signals with one, two, or three sources. 200 samples are taken for signals with different numbers of sources and marked with different labels. After random mixing, a training set with a total of 600 samples is formed. The training of the BP neural network is shown in Fig. 10: the error accuracy is set to 0.01; and after 963 times of learning, the training of the BP neural network model is completed.

1) DETECTION PROBABILITIES AGAINST DIFFERENT SNRS

The signal samples were collected in the RF anechoic chamber by the method of section B.(1). The setting of the experimental parameters is also the same as that of section B.(1). The detection probabilities of the six methods for one source and three source signals under different SNRs are shown in Fig. 11.

The trend of detection probability for each method in Fig. 11 is similar to that in Fig. 8. It should be noted that the signal data obtained from the RF anechoic chamber is different from the computer signal data. Because the former contains other colored noises from various types in the space. These noises will cause some errors in signal decomposition, which will affect the next step of source number enumeration. Therefore, compared with the Fig. 8, the detection probability of each method in the Fig. 11 dropped. However, the proposed method is still the best performer. Notably, when the number of sources is 3, other methods have failed or performed poorly

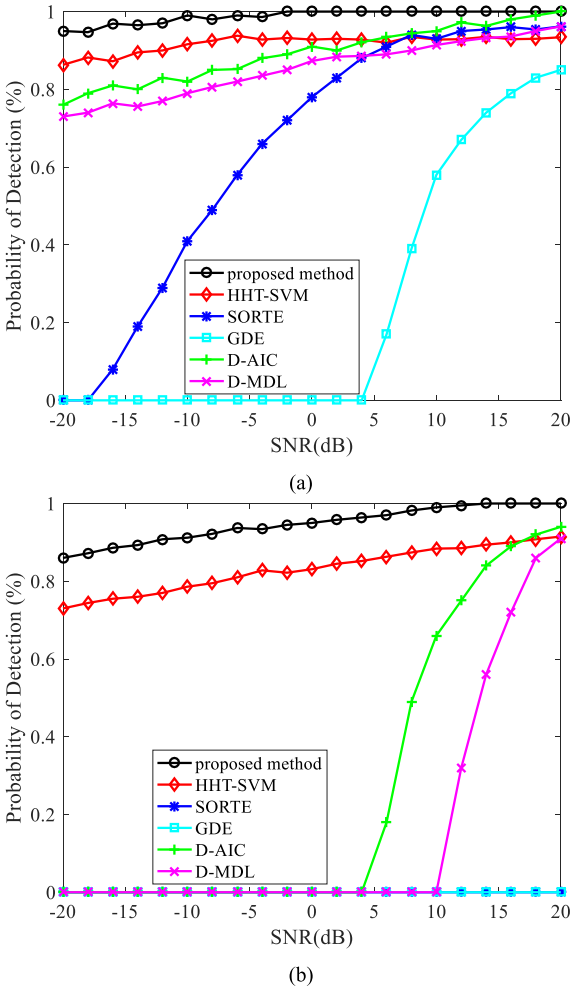

FIGURE 11. The detection probabilities of the six methods at different SNRs. (a) One source. (b) Three sources.

except for the proposed method and the HHT-SVM method. Besides the proposed method is even better than HHT-SVM in the whole SNR range. Therefore, the proposed method is more suitable for signal data in the real environment, and performs well under different SNRs.

2) DETECTION PROBABILITIES AGAINST DIFFERENT NUMBER OF SNAPSHOTS

This experiment used the signal samples collected in the RF anechoic chamber, and all parameters are the same as in section B.(2). Fig. 12 shows the detection probabilities of the six methods for one source and three sources signal under different snapshot numbers.

The trend of detection probability for each method in Fig. 12 is similar to that in Fig. 9. The analysis is similar to section C.(1). The proposed method performs the best compared to other methods regardless of whether it is under one source or three sources. It is worth noting that when the number of sources is 3 and the number of snapshots is 40, the detection probability of the proposed method exceeds 80%.

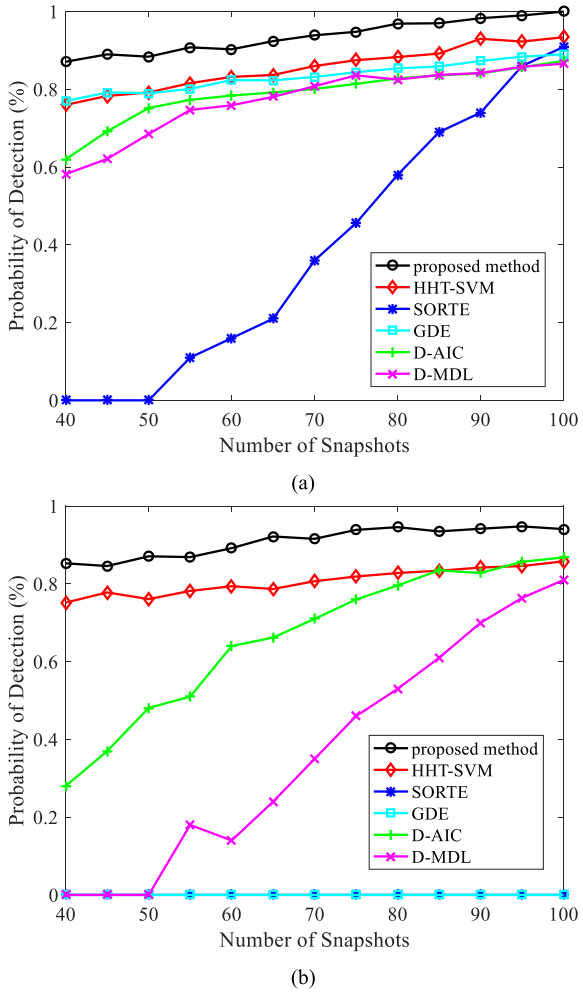

FIGURE 12. The detection probabilities of the six methods at different snapshots. (a) One source. (b) Three sources.

Therefore, the proposed method performs well under a small number of snapshots.

VI. CONCLUSION

This paper proposed an improved source number enumeration method based on SEMD. The proposed method addresses the end effect caused by cubic spline interpolation in EMD by extending the signal length. The source number enumeration method first obtains the instantaneous phase of the signal with HHT, where the EMD is replaced by the improved SEMD. The feature extraction is then performed on the instantaneous phase to obtain the feature vectors. To achieve high-dimensional eigenvectors, three differenct eigenvalues are added to the original eigenvectors. Finally, a special BP neural network is designed to predict the signal with an unknown number of sources. To evaluate the effectiveness of this source number enumeration method, a series of experiments are conducted in this paper. Firstly, SEMD and EMD are performed on the original signal, and the results obtained from both are compared. The result shows that SEMD can well restrain the end effect very well. Then, the experiment is carried out by comparing the proposed method with the HHT-SVM method, the SORTE method, the GDE method, the D-AIC method, and the D-MDL method. The experiment results show that the proposed method has a higher detection probability and better performance than other methods, especially when the number of sources is large or the number of snapshots is small. Finally, the data of the RF anechoic chamber is used to verify the effectiveness of the proposed method in the real environment. One limitation of the proposed method is that its computation is complicated. Therefore, optimizing the calculation is the future research direction of this work.

REFERENCES

[1] Q. Xie, X. Pan, J. Chen, and S. Xiao, "Joint DOD and DOA estimation for coherently distributed sources in bistatic MIMO radar based on joint diagonalization," *IEEE Access*, vol. 7, pp. 107805–107815, 2019.

[2] H. Lee, J. Ahn, Y. Kim, and J. Chung, "Direction-of-Arrival estimation of far-field sources under near-field interferences in passive sonar array," *IEEE Access*, vol. 9, pp. 28413–28420, 2021.

[3] A. Farahat and K. Hussein, "Dual-band (28/38 GHz) MIMO antenna system for 5G mobile communications with efficient DoA estimation algorithm in noisy channels," *Appl. Comput. Electromagn. Soc.*, vol. 36, no. 3, pp. 282–294, Apr. 2021.

[4] W.-J. Wu, R. Fan, C. Wang, and J. Wang, "A compact and anti-interference filter-antenna for modern wireless communication systems," in *Proc. IEEE 6th Int. Symp. Microw., Antenna, Propag., EMC Technol. (MAPE)*, Oct. 2015, pp. 60–62.

[5] Y. Qin and Y. Chen, "Signal processing algorithm of ship navigation radar based on azimuth distance monitoring," *Int. J. Metrol. Quality Eng.*, vol. 10, p. 12, Nov. 2019.

[6] R. Schmidt, "Multiple emitter location and signal parameter estimation," *IEEE Trans. Antennas Propag.*, vol. AP-34, no. 3, pp. 276–280, Mar. 1986.

[7] S. Haykin, J. Reilly, V. Kezys, and E. Vertatschitsch, "Some aspects of array signal processing," *IEE Proc. F Radar Signal Process.*, vol. 136, pp. 1–26, Feb. 1992.

[8] H. Clergeot, S. Tressens, and A. Ouamri, "Performance of high resolution frequencies estimation methods compared to the Cramer–Rao bounds," *IEEE Trans. Acoust., Speech, Signal Process.*, vol. 37, no. 11, pp. 1703–1720, Nov. 1989.

[9] J. Selva, "Computation of spectral and root MUSIC through real polynomial rooting," *IEEE Trans. Signal Process.*, vol. 53, no. 5, pp. 1923–1927, May 2005.

[10] T. Kailath, "ESPRIT-estimation of signal parameters via rotational invariance techniques," *Opt. Eng.*, vol. 29, no. 4, p. 296, 1990.

[11] M. Wax and T. Kailath, "Detection of signals by information theoretic criteria," *IEEE Trans. Acoust., Speech, Signal Process.*, vol. ASSP-33, no. 2, pp. 387–392, Apr. 1985.

[12] M. Wax and I. Ziskind, "Detection of the number of coherent signals by the MDL principle," *IEEE Trans. Acoust., Speech, Signal Process.*, vol. 37, no. 8, pp. 1190–1196, Aug. 1989.

[13] J. Guo, W. Huo, C. Fan, and H. Zhang, "A robust source enumeration algorithm for low SNR coherent signals based on eigenvectors," in *Proc. 3rd Int. Congr. Image Signal Process.*, Oct. 2010, pp. 3914–3918.

[14] A. Mariani, A. Giorgetti, and M. Chiani, "Designing ITC selection algorithms for wireless sources enumeration," in *Proc. IEEE Int. Conf. Commun. (ICC)*, Jun. 2015, pp. 4883–4888.

[15] L. C. Zhao, P. Krishnaiah, and Z. D. Bai, "Remarks on certain criteria for detection of number of signals," *IEEE Trans. Acoust., Speech, Signal Process.*, vol. ASSP-35, no. 2, pp. 129–132, Feb. 1987.

[16] A. Jian-Jian, L. Cheng-Cheng, and Z. Yong-Jun, "MDL algorithm for source enumeration using random matrix theory," *J. Signal Process.*, vol. 31, no. 2, pp. 187–193, 2015.

[17] H.-T. Wu, J.-F. Yang, and F.-K. Chen, "Source number estimators using transformed Gerschgorin radii," *IEEE Trans. Signal Process.*, vol. 43, no. 6, pp. 1325–1333, Jun. 1995.

[18] W. Chen, J. Reilly, and K. Wong, "Detection of the number of signals in noise with banded covariance matrices," *IEE Proc.-Radar, Sonar Navigat.*, vol. 143, pp. 289–294, Oct. 1996.
[19] Z. Lu and A. M. Zoubir, "Source enumeration in array processing using a two-step test," *IEEE Trans. Signal Process.*, vol. 63, no. 10, pp. 2718–2727, May 2015.
[20] J.-F. Cardoso, "Eigen-structure of the fourth-order cumulant tensor with application to the blind source separation problem," in *Proc. Int. Conf. Acoust., Speech, Signal Process.*, Apr. 1990, pp. 2655–2658.
[21] L. Yang, H. Zhang, J. Li, H. Yang, and Y. Cai, "Blind source enumeration based on Gerschgorin disk estimator and virtual array extension," in *Proc. 8th Int. Conf. Wireless Commun. Signal Process. (WCSP)*, Oct. 2016, pp. 1–4.
[22] A. K. Jain, J. Mao, and K. M. Mohiuddin, "Artificial neural networks: A tutorial," *Computer*, vol. 29, no. 3, pp. 31–44, Mar. 1996.
[23] J. Rogers, J. E. Ball, and A. C. Gurbuz, "Estimating the number of sources via deep learning," in *Proc. IEEE Radar Conf. (RadarConf)*, Apr. 2019, pp. 1–5.
[24] R. Fan, X. Zhu, W. Tang, and C. Si, "MFFNet: Multi-path features fusion network for source enumeration," *IEEE Commun. Lett.*, vol. 26, no. 3, pp. 572–576, Mar. 2022.
[25] W. Hu, R. Liu, X. Lin, Y. Li, X. Zhou, and X. He, "A deep learning method to estimate independent source number," in *Proc. 4th Int. Conf. Syst. Informat. (ICSAI)*, Nov. 2017, pp. 1055–1059.
[26] N. E. Huang, "The empirical mode decomposition and the Hilbert spectrum for nonlinear and non-stationary time series analysis," *Proc. Roy. Soc. London. Ser. A, Math., Phys. Eng. Sci.*, vol. 454, pp. 903–995, Mar. 1998.
[27] Q. Pan, C. Mei, N. Tian, B. W. K. Ling, and E. X. Wang, "Source enumeration based on a uniform circular array in a determined case," *IEEE Trans. Veh. Technol.*, vol. 68, no. 1, pp. 700–712, Jan. 2019.
[28] T. Xiong, Y. Bao, and Z. Hu, "Does restraining end effect matter in EMD-based modeling framework for time series prediction? Some experimental evidences," Neurocomputing 2014,123:174-184.
[29] O. B. Fosso and M. Molinas, "EMD mode mixing separation of signals with close spectral proximity in smart grids," in *Proc. IEEE PES Innov. Smart Grid Technol. Conf. Eur. (ISGT-Eur.)*, Oct. 2018, pp. 1–6.
[30] Y. Lei, Z. He, and Y. Zi, "Application of the EEMD method to rotor fault diagnosis of rotating machinery," *Mech. Syst. Signal Process.*, vol. 23, no. 4, pp. 1327–1338, May 2009.
[31] J. Li, C. Liu, Z. Zeng, and L. Chen, "GPR signal denoising and target extraction with the CEEMD method," *IEEE Geosci. Remote Sens. Lett.*, vol. 12, no. 8, pp. 1615–1619, Aug. 2015.
[32] Z. Tian, "Short-term wind speed prediction based on LMD and improved FA optimized combined kernel function LSSVM," *Eng. Appl. Artif. Intell.*, vol. 91, May 2020, Art. no. 103573.
[33] X. Zhang, Q. Miao, H. Zhang, and L. Wang, "A parameter-adaptive VMD method based on grasshopper optimization algorithm to analyze vibration signals from rotating machinery," *Mech. Syst. Signal Process.*, vol. 108, pp. 58–72, Aug. 2018.
[34] W. Hu, "DOA estimation for UCA in the presence of gain-phase errors," *IEEE Commun. Lett.*, vol. 23, no. 3, pp. 446–449, Mar. 2019.
[35] L. Pedroso, A. Arco, I. Figueiras, D. S. J. Araújo, J. Fernandes, and H. Lopes, "Application of cubic spline interpolation with optimal spatial sampling for damage identification," *Struct. Control Health Monit.*, vol. 29, Jan. 2022, Art. no. e2856.
[36] D. E. Rumelhart, G. E. Hinton, and R. J. Williams, "Learning representations by back-propagating errors," *Nature*, vol. 323, pp. 533–536, Oct. 1986.
[37] N. E. Huang, "Introduction to the Hilbert–Huang transform and its related mathematical problems," in *Hilbert–Huang Transform and its Applications*. Singapore: World Scientific, 2014, pp. 1–26.
[38] J. Benesty, "Adaptive eigenvalue decomposition algorithm for passive acoustic source localization," *J. Acoust. Soc. Amer.*, vol. 107, pp. 384–391, Jan. 2000.
[39] Y. Wu and H. C. So, "Simple and accurate two-dimensional angle estimation for a single source with uniform circular array," *IEEE Antennas Wireless Propag. Lett.*, vol. 7, pp. 78–80, 2008.
[40] Z. Shang-Yue, L. Yuan-Yuan, and Y. Gong-Liu, "EMD interval thresholding denoising based on correlation coefficient to select relevant modes," in *Proc. 34th Chin. Control Conf. (CCC)*, Jul. 2015, pp. 4801–4806.
[41] X. Jin, T. Qiu, and P. Wang, "New source number estimation algorithm based on L1 sparse regularization," *J. Commun.*, vol. 37, no. 10, pp. 75–80, 2016.
[42] Z. Zhen, J. P. Hu, Z. P. Huang, and Y. M. Zhang, "Estimation of source number for single-channel received signal," in *Proc. MATEC Web Conf.*, vol. 44, 2016, Art. no. 01064.
[43] H. T. Wu and C. L. Chen, "A new Gerschgorin radii based method for source number detection," in *Proc. 10th IEEE Workshop Stat. Signal Array Process.*, Aug. 2000, pp. 104–107.
[44] M. J. Chen, G. Q. Long, and Z. R. Huang, "Source number estimation in the presence of nonuniform noise," *J. Signal Process.*, vol. 2, pp. 134–139, Feb. 2008.

SHENGGUO GE received the B.S. degree from the Department of Physics and Optoelectronic Engineering, Guangdong University of Technology, Guangzhou, China, in 2016, and the M.S. degree from the Department of Information Engineering, Guangdong University of Technology, in 2020. He is currently pursuing the Ph.D. degree with Universiti Putra Malaysia. His research interests include signal processing, pattern recognition, and deep learning.

SITI NURULAIN BINTI MOHD RUM received the bachelor's degree from Universiti Teknologi Malaysia (UTM), the Diploma degree from Universiti Teknologi MARA (UiTM), and the master's and Ph.D. degrees from the University of Malaya (UM). She was an IT Practitioner for over 15 years and has been involved in various IT projects, administrations, and operations, specifically in software development and database development. She is currently a Senior Lecturer at the Department of Computer Science, Faculty of Computer Science and Information Technology, University of Putra Malaysia (UPM). She has published several journals and presented papers at the international conferences. She is actively involved in research and consultancy work in the IT field. Her research interests include but not limited to, the area in database processing, social media analytics, artificial intelligence, data science, and semantic web.

HAMIDAH IBRAHIM (Member, IEEE) received the Ph.D. degree in computer science from the University of Wales, Cardiff, U.K., in 1998. She is currently a Full Professor at the Faculty of Computer Science and Information Technology, Universiti Putra Malaysia (UPM). Her current research interests include databases (distributed, parallel, mobile, biomedical, and XML) focusing on issues related to integrity maintenance/checking, ontology/schema/data integration, ontology/schema/data mapping, cache management, access control, data security, transaction processing, query optimization, query reformulation, preference evaluation–context-aware, information extraction, concurrency control, and data management in mobile, grid, and cloud.

ERZAM MARSILAH received the B.Sc. degree in computer system from Universiti Putra Malaysia, in 2002, the M.Sc. degree in advanced computing (machine learning and data mining) from the University of Bristol, in 2006, and the Ph.D. degree in intelligent computing, in 2017. He has published on applications of machine learning in optimizing design of drugs and smart home environment. His research interests include machine learning and artificial intelligence specifically in reinforcement learning and evolutionary computing. His other interests include modeling creative and imaginative agents.

THINAGARAN PERUMAL (Senior Member, IEEE) received the Ph.D. degree in smart technology and robotics from Universiti Putra Malaysia. He is currently an Associate Professor with the Department of Computer Science, Faculty of Computer Science and Information Technology, Universiti Putra Malaysia. His research interests include towards interoperability aspects of smart homes and the Internet of Things (IoT), activity recognition for ambient intelligence, and cyber-physical systems. Some of the eminent works include proactive architecture for the IoT systems; development of the cognitive and semantic IoT frameworks for smart homes and activity recognition in smart environments. He is an Active Member of IEEE Consumer Electronics Society and its Future Directions Committee on the Internet of Things. He was a recipient of the 2014 Early Career Award from the IEEE Consumer Electronics Society for his pioneering contribution to the field of consumer electronics. He has received four best paper awards. He is currently appointed as the Chair of IEEE Consumer Electronics Society Malaysia Chapter. He has been invited to give several keynote lectures and plenary talks on the Internet of Things in various institutions and organizations internationally. He has delivered ten keynotes and served on five panels at various international conferences. His Scopus H-index is 16, with more than 1112 citations while Google Scholar H-index is 18, and i10-index is 19 with more than 727 citations.